

Water Resources Research



RESEARCH ARTICLE

10.1029/2018WR024541

Key Points:

- We demonstrate the capability of imaging full Darcy-scale experiments while obtaining pore-scale resolution
- In the mixed-wet system there is a difference between pore scale and Darcy scale production due to oil layers on the sample perimeter
- Water-wet systems show a clear imbibition front, whereas mixed-wet systems show only localized imbibition sites

Correspondence to:

W.-B. Bartels and H. Mahani,
willembart.work@gmail.com;
H.Mahani@shell.com

Citation:

Bartels, W.-B., Rücker, M., Boone, M., Bultreys, T., Mahani, H., & Berg, S. (2019). Imaging spontaneous imbibition in full Darcy-scale samples at pore-scale resolution by fast X-ray tomography. *Water Resources Research*, 55, 7072–7085. <https://doi.org/10.1029/2018WR024541>



Received 16 DEC 2018

Accepted 13 JUL 2019

Accepted article online 22 JUL 2019

Published online 22 AUG 2019

Imaging Spontaneous Imbibition in Full Darcy-Scale Samples at Pore-Scale Resolution by Fast X-ray Tomography

W.-B. Bartels^{1,2} , M. Rücker^{2,3} , M. Boone⁴ , T. Bultreys^{3,5} , H. Mahani² , S. Berg^{2,3} , S. M. Hassanizadeh¹ , and V. Cnudde⁵ 

¹Department of Earth Sciences, Utrecht University, Utrecht, Netherlands, ²Shell Global Solutions International B.V., Amsterdam, Netherlands, ³Department of Earth Science and Engineering, Imperial College London, London, UK, ⁴UGCT-PProGress, Ghent University, Ghent, Belgium, ⁵TESCAN XRE, Gent, Belgium

Abstract Spontaneous imbibition is a process occurring in a porous medium which describes wetting phase replacing nonwetting phase spontaneously due to capillary forces. This process is conventionally investigated by standardized, well-established spontaneous imbibition tests. In these tests, for instance, a rock sample is surrounded by wetting fluid. The following cumulative production of nonwetting phase versus time is used as a qualitative measure for wettability. However, these test results are difficult to interpret, because many rocks do not show a homogeneous but a mixed wettability in which the wetting preference of a rock varies from location to location. Moreover, during the test the flow regime typically changes from countercurrent to cocurrent flow and no phase pressure or pressure drop can be recorded. To help interpretation, we complement Darcy-scale production curves with X-ray imaging to describe the differences in imbibition processes between water-wet and mixed-wet systems. We found that the formation of a spontaneous imbibition front occurs only for water-wet systems; mixed-wet systems show localized imbibition events only. The asymmetry of the front depends on the occurrence of preferred production sites, which influences interpretation. Fluid layers on the outside of mixed-wet samples increase connectivity of the drained phase and the effect of buoyancy on spontaneous imbibition. The wider implication of our study is the demonstration of the capability of benchtop laboratory equipment to image a full Darcy-scale experiment while at the same time obtaining pore-scale information, resolving the natural length and time scale of the underlying processes.

1. Introduction

Spontaneous imbibition is the predominantly capillary-driven invasion of wetting phase into the pore space of a porous medium saturated with nonwetting phase. This process is seen in daily life, for instance, when coffee infiltrates cookies or when ink infiltrates paper (Alava et al., 2004; Gruener et al., 2012; Miranda et al., 2010). It is relevant in various geological applications including soil infiltration (De Rooij, 2000; Xiong, 2014), CO₂ storage (Bickle, 2009; Juanes et al., 2006), environmental remediation—in which nonaqueous phase liquids (NAPLs) are to be removed—(Brusseau, 1992; O'Carroll et al., 2010), and petroleum engineering (Blunt et al., 2002). Spontaneous imbibition occurs in these examples during unsteady state displacement, where capillarity leads to an invasion front (Gruener et al., 2012).

The impact of capillary forces on a fluid-fluid-solid system is quantified by capillary pressure-saturation curves, which consist of a forced part and a spontaneous part. The spontaneous part is typically measured in tests such as the Amott spontaneous imbibition test (Amott, 1959; Donaldson et al., 1969). An Amott test provides a value for the saturation at a capillary pressure of zero by measuring the cumulative fluid production versus time (Fischer & Morrow, 2005; Graue et al., 1999; Tang & Morrow, 1997; Zhou et al., 2000).

This production curve can be used in combination with information from the capillary pressure-saturation curve to characterize wettability of a specific fluid-fluid-rock system on the core scale (Suijkerbuijk et al., 2013). Such an assessment is often accompanied by the assignment of an Amott index or USBM index. Wettability is a property of a multiphase system (here two liquids and a solid) that describes the preference of one fluid to be in contact with the solid over another. It is known to impact the flow behavior of the two fluid phases significantly in the porous medium (Anderson, 1987; Blunt, 2001; Rücker et al., 2019). In

©2019. The Authors.

This is an open access article under the terms of the Creative Commons Attribution License, which permits use, distribution and reproduction in any medium, provided the original work is properly cited.

water-wet rock, the relative permeability of the nonwetting fluid (air, CO₂, NAPL, or oil) is larger than in mixed-wet rock, implying that more fluid can be recovered in shorter times (Anderson, 1987; Blunt, 2001; Picchi & Battiato, 2018; Zou et al., 2018). However, in mixed-wet rock, the residual saturation of the produced fluid is significantly lower than in water-wet rock, meaning that over longer times the ultimate recovery in mixed-wet systems may be higher than in water-wet systems. Therefore, an accurate representation of the wettability of a rock type and the fluids it contains is imperative in predicting flow dynamics.

Other factors that affect the cumulative production versus time curves in Amott tests can complicate the assessment of wettability. Such factors are initial water saturation, mobility and viscosity, interfacial tension variations, sample dimensions, and the physics (cocurrent or countercurrent) of imbibition that is occurring (Cai et al., 2012; March et al., 2016; Schmid & Geiger, 2012; Weisbrod et al., 2009).

To correct for those factors, different scaling groups have been proposed (Mattax & Kyte, 1962, 1997; Schmid & Geiger, 2012, 2013). These scaling groups have been effective for interpreting many cases of uniform wettability (Ma et al., 1997); however, some natural systems are believed to be mixed wet (Salathiel, 1973). One reason for this is chemical heterogeneity of the rock. The different minerals within a rock may interact differently with the fluids present. Another reason could be wettability alteration. Fluids such as NAPL or crude oil may react or adsorb on the surface of the rock, which results in a change in wettability (Lee et al., 2007; Morrow et al., 1986; Powers et al., 1996). In some locations of the pore space connate water may prevent direct contact between fluid and the rock surface causing inhomogeneous wettability alteration and consequently a mixed-wet state. Additionally, wettability indices are often misleading when it comes to predicting sample wettability or the associated flow behavior (Dixit et al., 1999), since they are nonunique measures of wettability and are applied to systems that depend on spontaneous processes and self-controlled dynamics.

In summary, the wettability index that followed from curves of total production versus time may not reflect the wettability following from the sum of the local pore space wettability states, at least for mixed-wet systems. Since wettability is defined by parameters below the core scale, this finding is not necessarily surprising. From the point of view of displacement physics, spontaneous imbibition tests are notoriously difficult to interpret because the pore-scale flow regimes typically change from initially countercurrent flow to cocurrent flow (Fernø et al., 2015; Mason & Morrow, 2013). Here, the latter may not only be driven by capillary forces but may also be influenced by gravity.

To make spontaneous imbibition experiments interpretable with Darcy-scale models, additional boundary conditions are needed. Some studies aim at experimentally controlling the boundary condition, for instance, having only the two end faces of the sample open and each face exposed to a different fluid phase (Haugen et al., 2014; Mason & Morrow, 2013). Additionally, pressure measurements of (both) fluid phases and ideally also saturation monitoring are preferred (Fernø et al., 2015; Mason & Morrow, 2013; Mason et al., 2010; Zahasky & Benson, 2019). However, that requires additional experimental effort, which deviates significantly from the standard Amott test and therefore is usually not taken. Therefore, the challenge remains to understand what the actual boundary condition is and its impact on the flow dynamics.

Moreover, besides the issue with the boundary conditions, numerical simulators struggle to reproduce the flow regimes of spontaneous imbibition, in particular the countercurrent regime.

One of the main reasons is that in Darcy-scale simulators, typically only the domain inside the rock is captured and then boundary conditions must be imposed. However, in the experiment these boundary conditions evolve dynamically which is not that obvious from a Darcy-scale perspective, where typically at all open faces a “capillary pressure equal to zero” ($P_c = 0$) boundary condition is applied. Detailed experiments show that the expelled nonwetting phase forms small bubbles at the outside of the sample that generate a capillary back pressure, which needs to be considered for the production of the nonwetting phase (Unsal et al., 2009; Unsal, Mason, Morrow & Ruth 2007; Unsal, Mason, Ruth & Morrow 2007).

When approaching this problem using pore-scale simulators, we know that such simulators cover the pore-scale processes correctly. Therefore, the unknown is in the wetting boundary condition at the solid and the flow boundary condition at the outside of the sample, which need to be specified as input to solving the set of partial differential equations. In these pore-scale simulators the wetting boundary condition is usually expressed through contact angles. These can be obtained either from model fluid-fluid-solid systems (Morrow, 1975; Morrow et al., 1986) or directly in the rock using micro-CT imaging (Andrew et al., 2014a). However, while model systems miss the full complexity of the fluid-fluid-rock system, in situ contact angle

measurements are difficult to interpret as the detected contact angles depend on unknown measurement conditions, such as the current status of the interface (advancing or receding) or subpore-scale heterogeneity (chemical and structural). In the end, wettability is the parameter that will be estimated or matched from experimental investigations. So the entire uncertainty is on the flow boundary condition on the outside of the sample, which is one of the focus areas of this study.

Still, interpretation of the production curves and consequently wettability may be improved by pore-scale information (Mason & Morrow, 2013). For instance, knowledge of fluid connectivity inside the pore space allows the estimation of the gravity head, the distinction of capillary-driven spontaneous processes from other effects, and insight into the conceptual differences of spontaneous imbibition in water-wet rock or mixed-wet rock.

The pore-scale information could also be used for validation of experimental protocols; capillary end effects or trapped gas can be detected, which are known to impact spontaneous imbibition significantly. For that purpose we prepare a sample such that we have a known wettability distribution to remove that from the list of unknowns to focus on the preparation protocol and its impact on the observation and respective interpretation.

Pore-scale imaging offers a tool to investigate these processes; however, one of the main challenges has always been the very limited field of view (FOV) of micro-CT at resolutions sufficient to image the pore-scale fluid distribution; see, for instance, Alizadeh et al., 2017, (2017). This needs to be done accurately enough to assess connectivity and perhaps also to assess curvature of the liquid-liquid interface as to estimate capillary pressure (Andrew et al., 2014b; Armstrong, Porter & Wildenschild 2012; Armstrong, Pentland, et al., 2012; Chaudhary et al., 2013; Lv et al., 2017).

The necessity of visualizing a sample of that magnitude and at such a high resolution ties into the forces that are involved in the spontaneous imbibition experiments: capillary, viscous, inertial, and gravity forces. Capillary and inertial forces would largely be covered at the scale of individual pores. Viscous forces scale with flow, and the length scale at which viscous forces typically become larger than capillary forces is at the scale from millimeter to centimeter (Armstrong et al., 2014). Finally, the scale at which gravity exceeds capillary forces occurs at several centimeters. That is the scale ultimately responsible for the transition of an initially countercurrent imbibition to cocurrent imbibition, hence an important scale in the spontaneous imbibition problem as indicated in the previous sections. This last transition is the main reason why we need a sample of several centimeters length in order to be sure that we cover the larger-scale dynamics correctly, that is, the scale that defines the predominant pressure gradient during cocurrent flow, which is particularly relevant for the mixed-wet condition where larger-scale connectivity may be present leading to film flow. Novel micro-CT technology enables combining Darcy-scale sample sizes with pore-scale resolution (Cnudde & Boone, 2013; De Kock et al., 2015) and therefore allows the investigation of all four forces involved in the spontaneous imbibition process.

In this study, we use core plugs typically used in special core analysis (SCAL, dimensions of 5 cm in length and 2.54 cm in diameter) to assess the benefit of using micro-CT imaging as a pore-scale validation tool. In addition, we used fast, laboratory benchtop micro-CT imaging to determine the underlying pore-scale processes of spontaneous imbibition (Bultreys et al., 2015; Bultreys, Boone, et al., 2016; Van Stappen et al., 2014). The visualized volume contains both the sample and the surrounding fluid, making this a suitable data set for pore-scale simulation of spontaneous imbibition processes as suggested by Mason and Morrow (2013).

We need time-resolved 3-D information at pore-scale resolutions for Darcy-scale samples (i.e., SCAL samples that fulfill the size requirements and assumptions for applying Darcy's law), which recently has been made available in the laboratory without the need for synchrotron beamline facilities by the Centre for X-ray Tomography of Ghent University (www.ugct.ugent.be) in collaboration with TESCAN XRE (www.xre.be). Three novel apparatuses (a microcoreholder, an X-ray transparent Amott cell for Darcy-scale plugs, and an additional one for miniplugs; see Figure 3) were used together with HECTOR and Environmental Micro-CT scanner (EMCT; Bultreys, De Boever & Cnudde 2016; Dierick et al., 2014). The combination of the monitored pore-scale behavior and the observed cumulative oil production versus time curves provides a better understanding of the underlying processes of spontaneous imbibition.

Table 1
Composition of FW

Ion	Value (g/L)	Ion	Value (g/L)
Na ⁺	49.9	Cl ⁻	112
Mg ²⁺	3.25	SO ₄ ²⁻	0.234
Ca ²⁺	14.5	HCO ₃ ⁻	0.162

Note. Total dissolved solids (TDS) = 180 g/L and ionic strength = 3.659 mol/L. FW = formation water.

A particular requirement for using X-ray in spontaneous imbibition experiments is that not only the core holder but also the fluid in which the sample is immersed should be X-ray transparent. Therefore, this fluid phase cannot be doped something one may overlook when attempting to repeat the experiment.

2. Materials and Methods

2.1. Fluid-Fluid-Rock System

We used formation water (FW, density $\rho = 1.152\text{g/cm}^3$, viscosity $\mu = 1.550\text{ mPa}\cdot\text{s}$, at $T = 20^\circ\text{C}$, composition; see Table 1), decane ($\rho = 0.730\text{ g/cm}^3$, $\mu = 0.920\text{ mPa}\cdot\text{s}$, at $T = 20^\circ\text{C}$), and crude oil ($\rho = 0.8833\text{ mPa}\cdot\text{s}$, $\mu = 11.486\text{ mPa}\cdot\text{s}$, at $T = 20^\circ\text{C}$, composition; see Table 2) for the experiments. Both decane and crude oil were doped with 20 wt% Iododecane to obtain higher X-ray attenuation. As rock we used a carbonate (Oolite) rock (Muir-wood, 1952), Ketton, with a porosity of $\phi_{\text{MICP}} = 23\%$ and a brine permeability of $K_{\text{brine}} = 5.7\text{ E-}12\text{ m}^2$.

Information about the crude oil-brine-rock systems together with their desaturation method can be found in Table 3. We used two types of plugs: Darcy-scale plugs (5-cm length and 2.54-cm diameter; pore volume $V_p = 5.83\text{ ml}$) and miniplugs (20-mm length and 4-mm diameter; pore volume $V_p = 57.8\text{ }\mu\text{l}$).

The miniplugs would easily break when crafting them from larger rock specimen, and those that survived are therefore more likely to contain a larger fraction of cement, also compared to the Darcy-scale plugs. The cement can make up 40% of the total porosity in Ketton (see Figure 1) and contains, for the micro-CT scanners and settings used in this study, unresolvable microporosity. This is consistent with the initial water saturations for the Darcy-scale plugs based on centrifuge data shown in Table 3. Based on the centrifuge data overlaying the pore size distribution in Figure 1, microporosity was not filled with doped (crude) oil in which case the role of the water saturated microporosity is limited to slightly increasing the water connectivity.

2.2. Sample Saturation

The Darcy-scale and mini-plugs were placed in a sleeve in a desiccator in which a vacuum ($\sim 10^{-2}\text{ mbar}$) was created. Subsequently, the samples were saturated by adding de-aerated FW to the desiccator. To dissolve any gas bubbles that may have been left behind in the pore space, all samples were submerged in de-aerated brine in a bottle sealed off by a rubber stopper and exposed to 30 bars of pressure for 2 hrs.

2.3. Sample Desaturation: Centrifuge and Micro-Core Holder

The Darcy-scale plugs were brought to initial water saturation in a centrifuge (URC-628, Coretest Systems Inc., used at 3,500 RPM for Darcy-scale plugs) in 24 hrs. The temperature was constant at 40°C to counter the gradual heating during centrifuging that usually occurs. The connate saturations shown in Table 3 were computed by combining the automatic recording of the production and a material balance calculation.

In Figure 2, a saturation profile was computed for the conditions of the centrifuge experiment at given speeds and capillary pressure saturation for the rock in this study (Wang & Masalmeh, 2019). It is based on the balance of capillary forces and centrifugal forces in the centrifuge. The saturation gradient is based on the

Table 2
Crude Oil Properties: Interfacial Tension (IFT), Total Acid Number (TAN), Total Base Number (TBN), and Asphaltene Content

IFT FW/doped crude oil	TAN (mg KOH/g)	TBN (mg KOH/g)	Asphaltenes (g/100 ml)
20 mN/m at 20°C	0.5	1.0	0.244

Note. FW = formation water.

Table 3
List of Samples Used in This Paper

Sample	Oil phase	S_{wi}	Desaturation	Aging	Wetting
KET06	Decane	0.37	Centrifuge	40 °C/24 hr	Water wet
KET08	Crude oil	0.34	Centrifuge	40 °C/24 hr	Mixed wet
KET09	Crude oil	0.38	Centrifuge	40 °C/24 hr	Mixed wet
Miniplug	Crude oil	0.06	Flooding	40 °C/24 hr	Water wet

Note. We used two types of plugs: small Darcy-scale plugs (5-cm length and 2.54-cm diameter) and miniplugs (20-mm length and 4-mm diameter), both Ketton rock. The initial water saturation (S_{wi}) excludes the water in the micropores for the miniplug. The oil phases were doped with 20 wt% Iododecane.

well-known capillary end effect (Huang & Honarpour, 1998) caused by a zero capillary pressure boundary condition at the production face of the rock. The capillary end effect is minimal.

Centrifugation at elevated temperature caused aging of doped crude oil saturated rock even in this short time, which will be further explained in sections 3.1 and 3.2. Aging occurs were the oil gets in contact with the rock surface (Kovscek et al., 1993). As only the large pores got filled with oil during drainage, the small pores remain water wet (Figure 1). This lead to two mixed-wet Darcy-scale plugs saturated with doped crude oil and one water-wet Darcy-scale plug saturated with doped decane; see Table 3.

The miniplug samples were desaturated by flooding in the specially designed micro-core holder; see Figure 3a. The core holder consisted of Hastelloy steel and X-ray transparent PolyEther Ether Ketone (PEEK), which meant that the saturation state of the sample could be monitored during and after (de)saturation. A steel pressure vessel that regulated the sleeve pressure was situated at the bottom of the cell. The pressurizing fluid was distilled water (up to 30 bars). Because of the pressure vessel there was no need to keep any pressure line attached to the setup. The micro-core holder could be used for both static (e.g., aging tests) and dynamic (e.g., flow tests) experiments at elevated temperatures up to 80 °C. Properties of the miniplug can be found in Table 3.

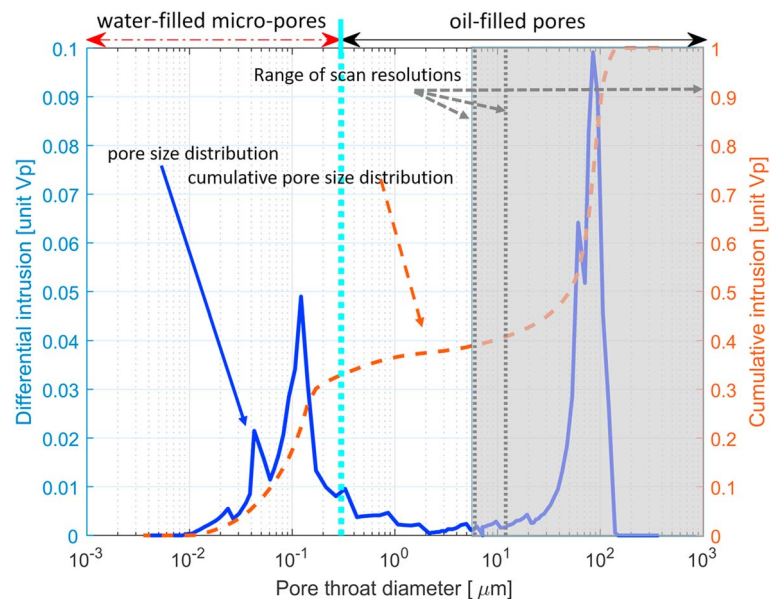


Figure 1. Mercury intrusion curve of one of the Darcy-scale Ketton samples. The black dotted lines indicate the voxel resolutions of different scans that were made. The grayed-out area shows the maximum portion of the pore size distribution that was visualized in this work. The blue dashed line indicates the smallest pores filled with crude oil by the centrifuge (the range is indicated by the solid black arrow at the top). All scans capture the larger pores and are well above the sizes of the water-filled microporosity (indicated by the red dash-dotted arrow at the top).

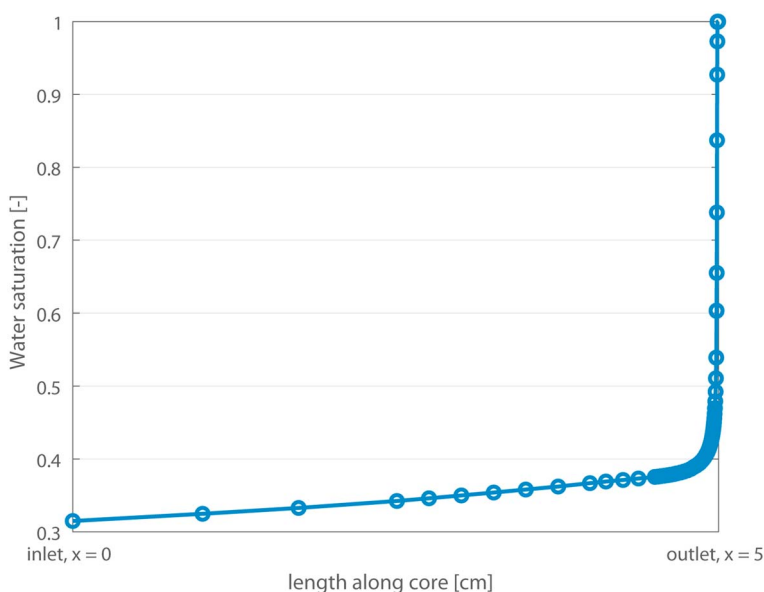


Figure 2. The estimation of the capillary end effect along the length of the Darcy-scale plug.

2.4. Experimental Protocols

We used standardized experimental protocols for spontaneous imbibition tests as conducted in the oil and gas industry. An exception was the aging for Darcy-scale plugs as addressed above. One step in the Darcy-scale plug Amott protocol is to roll the sample on a tissue saturated with the fluid present in the rock to remove fluid attached to the outside of the sample (Amott, 1959). However, this may create suction on the surface pores if the tissue is not wet enough, or it may not remove all fluid from the outside of the sample when the tissue is too wet. Both scenarios may influence the cumulative production versus time curve. Still, it was decided to adhere to the standard protocols. For the miniplug, similar protocols were used. However, because of the small volume of resolvable pore space and because the production was not measured, it was decided to refrain from rolling the sample. In addition, because spontaneous imbibition may be a subsecond process, it is relevant to note that the delay between filling the cells with brines and starting of the scans was around 1 min for the miniplugs and around 5 min for the Darcy-scale plugs.

2.5. Spontaneous Imbibition Setups

Two different apparatuses were used for spontaneous imbibition: one for the Darcy-scale plug Amott tests (a slightly modified standard Amott cell; Figures 3b and 3d) and one for the miniplug Amott test; see Figures 3c, 3e, and 3f. The cells can handle samples of various sizes. Both cells can be used for spontaneous imbibition tests with different boundary conditions, that is, different parts and different amounts of the sample perimeter that are exposed to the surrounding brine. The cells are made of oil-resistant and X-ray-transparent materials. For all faces open spontaneous imbibition tests, the rock sample needs to be well consolidated. Other types of imbibition experiments (one end open or two ends open) are possible when a sleeve is used, which also poses less stringent requirements on the consolidation state of the sample. The boundary conditions influence whether cocurrent or countercurrent spontaneous imbibition processes occur and therefore influence the outcome of the experiments.

The sample holders, depicted in Figures 3b and 3c, that are placed in the cell are constructed to minimize contact with the sample while simultaneously fixing the sample position in the cell. It is vital that the samples do not move during the scans to prevent blurring of the images. In the case of the Darcy-scale plugs, the points where the sample holder touches the sample were made of water-wet glass to prevent oil from spreading along the holders.

2.6. Micro-CT Scanners: HECTOR and EMCT

HECTOR (Dierick et al., 2014) was used for time lapse imaging of the Darcy-scale plugs. The X-ray tube was operated at 160 kV with a power of 14 W. The plug was imaged using four consecutive scans along the vertical axis of the sample, which were merged together, resulting in a total reconstructed volume of

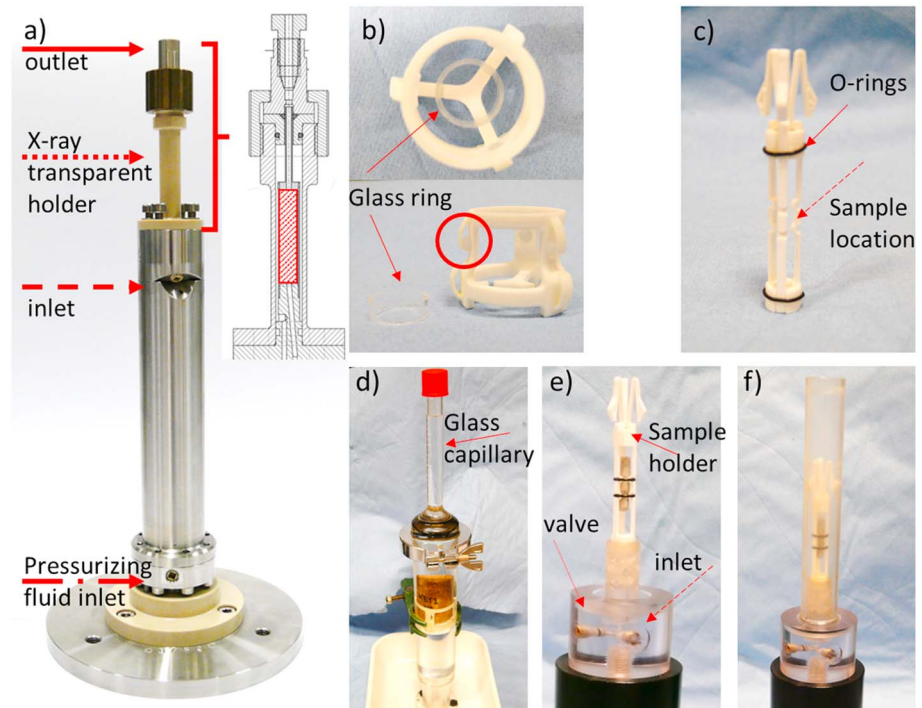


Figure 3. (a) Microcoreholder for desaturation of miniplugs and flow experiments. The bottom cylinder is a pressure vessel, with water as pressurizing agent. The polyether ether ketone top holds the sample and allows for X-ray scanning. This section is shown again in the inset in which a typical miniplug (4 mm × 20 mm) is indicated by the red square. Flow lines for desaturation can be attached at the top and bottom of the section. Sample holders for the spontaneous imbibition cells (b, c) and the spontaneous imbibition cells for Darcy-scale plugs (d) and miniplug (e, f).

2,000 × 2,000 × 4,700 voxels, with a voxel size of 14.25 μm. Individual consecutive scans were used to reduce the scan time (100 min per scan) and limit motion blurring during the acquisition.

EMCT (Bultreys, De Boever & Cnudde 2016) was used for fast dynamic imaging of the miniplugs. Unlike conventional micro-CT systems, the sample remains immobile in the EMCT, while the X-ray tube and detector rotate around the samples in a horizontal plane. This fixed sample configuration makes the system ideal for continuously monitoring dynamic in situ processes. The miniplugs were imaged at different spatial and temporal resolutions related to the assumed rate of the process that was monitored. The onset of the imbibition was imaged with a high temporal resolution of 15 s for a full rotation and a spatial resolution of 13 μm. Later stages of the process were imaged at a spatial resolution of 6.7 μm and a temporal resolution down to 70 s for a full rotation.

In Figure 1, the spatial resolution obtained by imaging are compared to the characteristic features in the pore size distribution, that is, range of macroporosity and microporosity.

2.7. Image Analysis

All scans were reconstructed (filtered back projection) using the dedicated reconstruction tools in the Aquila software package from TESCAN XRE. The large FOV was acquired by stitching images together. Further postprocessing and visualization of the data were done using Avizo 9.2.0 (ThermoFisher Scientific) and GeoDict (Math2Market). The images were first filtered with a nonlocal means filter and subsequently segmented by comparing the data of the dry scan, that is, the scan of the rock material without any fluids, with the wet scans captured during the spontaneous imbibition experiment, following the procedure described in Berg et al. (2014).

We observed a considerable amount of cement in the matrix in the micro-CT images, giving rise to a large fraction of microporosity which may influence the results. The cement is difficult to identify in wet samples, because the attenuation is close to that of the oil phase. However, by subtracting dry scans, it is still clear which parts of the FOV should be considered as pore space.

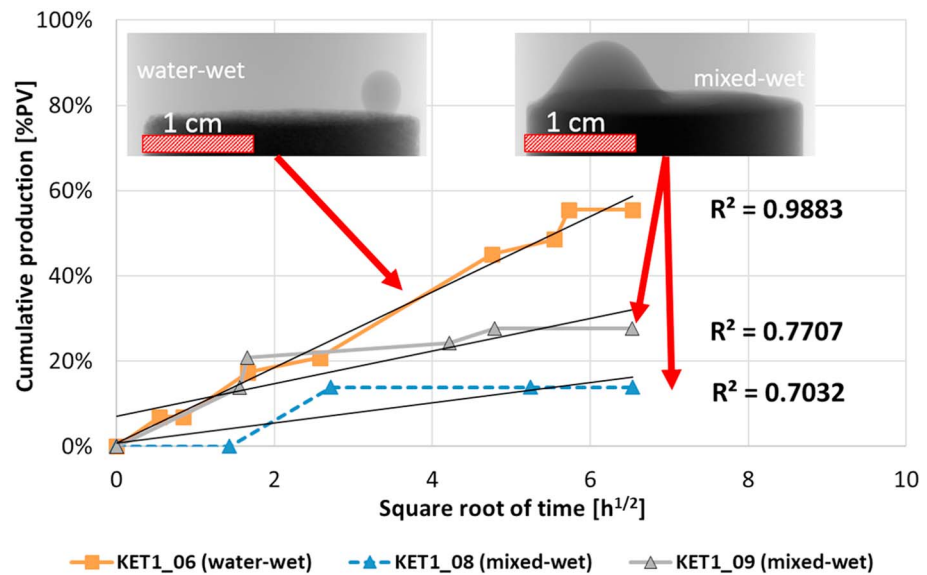


Figure 4. Oil production, given in percentage of visible pore volume, for both water-wet and mixed-wet samples, occurs right after immersion in brine. For the water-wet sample KET06 the imbibition rate and the square root of time were linear, which is in agreement with the Lucas-Washburn equation. KET08 was kept for a total of 122 days in which no additional production occurred. The reconstructed images show drop shapes that depend on wettability; a larger version of those images can be found in Figure 5.

3. Results and Discussion

3.1. Differences Between Pore Scale and Macroscopic Production in Darcy-Scale Samples

In Figure 4, the cumulative production versus time for three Ketton Darcy-scale samples is shown. The wettability of the samples relative to each other is clear: the water-wet sample shows more production than both mixed-wet samples as would be expected on these timescales.

Additionally, wettability states are confirmed from the shape of the droplets appearing on top of the samples as shown in the reconstructed images of both samples in Figure 4. In the water-wet sample droplets are produced and snap-off from the top, whereas the drop produced from the mixed-wet sample is static and shows more spreading, with a larger contact angle indicative of oil adhesion on the rock surface.

Micro-CT imaging can be used to find the origin of the macroscopic production inside the rock. Based on the obtained images, pore size distributions and fluid distributions were computed to assess whether the production originates predominantly from larger or smaller pores. The comparison between the initial and final crude oil distribution within the pore space shows a total volume difference of only 1% in the mixed-wet case. This cannot explain the macroscopically observed cumulative production curve of approximately 1 ml in Figure 4.

In other words, the volume balance that should exist between the macroscopic production and the change in pore occupancy is not fulfilled. The pore-scale observations show directly that the cumulative production by itself may not be sufficient to assess wettability states. The reason for this mismatch will be discussed in the following sections by describing the fluid motion in the pore space.

3.2. Dynamics of Oil Production at the Pore Scale

Micro-CT imaging provides additional information for wettability assessment besides the cumulative production versus time curves. As indicated in section 3.1, droplets appearing from the samples seem to reflect the wettability state too: the more rounded the shape, the more water wet the wettability state of the surface of the sample is. Figure 5 shows how the wettability state of the droplets on the surface is reflected in the pore space of the rock.

Two distinctly different forms of spontaneous imbibition occur. In the water-wet samples (Figures 5a, 5b, and 5e), we observe the formation of preferential production sites. Droplets form repeatedly at the same location at the top of the sample as indicated in Figure 5a. However, after a while this site stopped producing and a new production site emerged at the sample side just below the FOV. On the pore scale an asymmetric

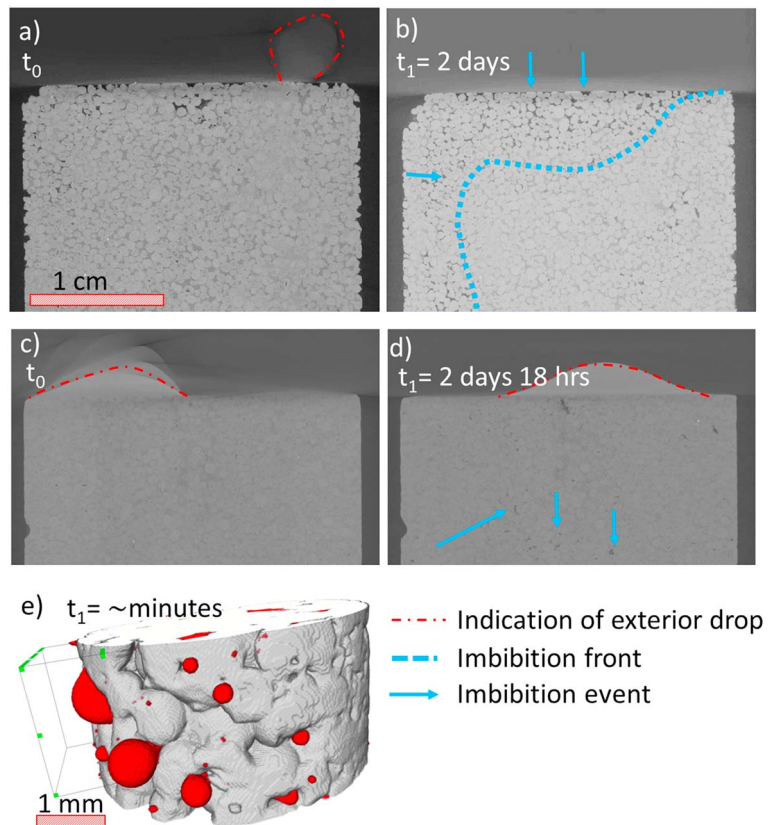


Figure 5. (a) The initial saturation of the water-wet Darcy-scale sample at $t_0 \approx 105$ min. (b) The saturation after 2 days for the water-wet Darcy-scale sample. A clear imbibition front has formed, indicated by the blue line and arrows. Note: the blue line and arrows are meant to guide the eye and were not derived by analysis. The center of the sample shows very little change. In (c), the initial saturation of the mixed-wet Darcy-scale sample is shown at $t_0 \approx 105$ min. (d) Almost no change in the mixed-wet sample after ≈ 2 days, except for some little changes indicated by blue arrows. (e) The drops emerging from the miniplug show mainly water-wet characteristics, even though it received similar treatment as the mixed-wet sample. Compare the shape of the droplets in (e) with that of the droplets emerging in (a), (c), and (d).

spontaneous imbibition front is observed in the water-wet Darcy-scale sample. A similar observation was reported for forced drainage, which represents the inverse process, by Berg et al. 2013.

The asymmetry is an unexpected phenomenon, since access to the pore space is limited only by the wetting state of the sample and the pore diameter. Hence, for a homogeneous rock such as Ketton, an inward moving circular front along the length of the sample is expected (Mason et al., 2009). In the mixed-wet Darcy-scale sample (Figures 5c and 5d), spontaneous imbibition seems to occur as isolated fluid phase changes throughout the sample. However, as indicated before (section 3.1), those filling events are not sufficient to explain the overall production at the macroscopic scale.

The displayed micro-CT images in Figure 5 show only the top part of the samples. Therefore, high cumulative production might be explained by spontaneous imbibition processes occurring in the bottom part of the sample. Visualization of the entire sample in Figure 6a shows that this is not the case and that the fluid saturation seems to be homogeneously distributed throughout the sample with very little fluid displacement.

In short, though the relative magnitude of spontaneous imbibition is reflecting both wettability states correctly as shown by the cumulative production curves in Figure 4, the absolute magnitude of the cumulative production cannot be explained by pore-scale events alone. Therefore, the roles of sample protocols and buoyancy are investigated in the following sections.

3.3. Artifacts Introduced by Standard Sample Handling and Experimental Protocols

Commonly, the experimental procedure for spontaneous imbibition Amott tests consists of taking a saturated and subsequently desaturated sample after aging and rolling it over a tissue wetted with the assessed

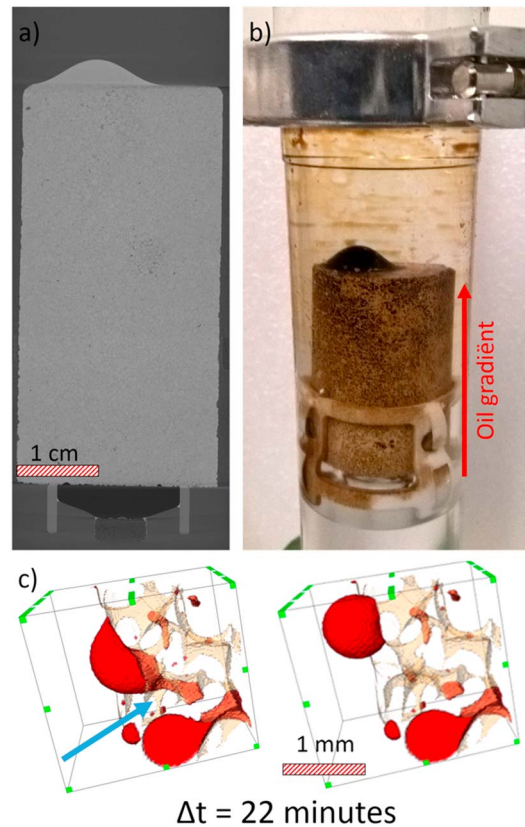


Figure 6. (a) Micro-CT scan of the full length of the Darcy-scale plug, after 2 days in spontaneous imbibition. Very little imbibition occurred via the isolated fluid phase changes. (b) Oil covering the perimeter of the sample; in the vertical direction there seems to be a gradient in oil coverage (more oil at the top than the bottom) not related to the white sample holder. (c) Upward movement and snap-off of an oil cluster at the water-wet miniplug perimeter 22 min apart.

fluid (Amott, 1959); see also section 2.4. From the pore-scale images it seems that no oil was removed due to suction during this step; however, in Figure 6b an oil layer can be seen adhering to the sample perimeter.

To investigate the effect of rolling on the production curves, one experiment with and one without rolling the sample was conducted. This could be at least part of the reason for the difference between the curves for the mixed-wet samples in Figure 4, which means that the rolling procedure has a large impact on the cumulative production curves and potentially also on the wettability indices derived thereof.

In Figure 6b, one of the Darcy-scale samples (KET09) is shown during the Amott test. In this example, a layer of oil of varying thickness on the cylindrical part of the sample is assumed to be the remainder of the initial oil layer covering the perimeter that has contributed to the macroscopic production.

A layer of approximately 250 μm covering the sample perimeter excluding top and bottom at the start of the experiment would be already enough to explain 1 ml of observed production if it is recovered in its entirety. This layer thickness was estimated by assuming a cylindrical sample with a uniform oil layer, covering the entire sample except the top and the bottom; see equation (1)

$$t_{\text{layer}} = \sqrt{\frac{V_{\text{prod}}}{h\pi} + r_{\text{sample}}^2} - r_{\text{sample}} \quad (1)$$

in which t is the layer thickness (cm), V_{prod} the produced volume of oil (ml), h the sample height (cm), and r_{sample} the sample radius (cm).

An additional effect of the occurrence of such a layer is that it increases both the connectivity of the oil phase and the gravity head.

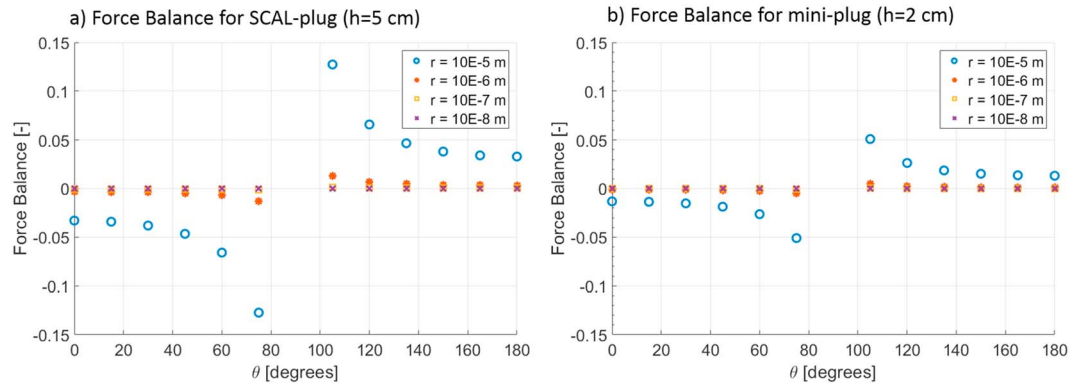


Figure 7. (a) Force balance for the Darcy-scale plug based on equation (2) and values in Tables 1 and 2. (b) Force balance for miniplug based on equation (2) and values in Tables 1 and 2. When the density difference is negative, F_b points in the opposite direction as the gravitational acceleration g . The negative sign is compensated by $\cos(\theta)$ for angles larger than 90° . SCAL = Special Core Analysis.

The discussion above suggests that sample handling and experimental protocols may have an effect on the most important variable that is measured during standard spontaneous imbibition tests, which is the cumulative production versus time as already shown in Figure 4.

This means that the sensitivity of these experiments to the standard protocol is very large and should be considered when interpreting results.

3.4. The Significance of Buoyancy for Spontaneous Imbibition Processes

A fundamental question when interpreting spontaneous imbibition experiments is if the observed processes are buoyancy (gravity) or capillary driven. A scaling analysis may answer this question. However, without detailed knowledge of the pore-scale fluid connectivity, the height of the gravity head needs to be assumed.

In Figures 5a, 5c, and 6 there seems to be a tendency for oil to migrate upward along the surface and/or leave the sample from the top implying a buoyancy effect. Usually, buoyancy is deemed unimportant in spontaneous imbibition in small samples of geological porous media on nongeological time scales. The main reason is the (usually) small pore size of those materials, which cause capillary forces to dominate. However, Ketton has a wide range of pore sizes that incorporate diameters of tens to hundreds of micrometers indicated in Figure 1. The scans in this study provide both local estimates of pore sizes and an opportunity to directly measure the height of the gravity head.

To investigate the effect of buoyancy, the force balance between buoyancy and capillary forces was computed; see Figure 7 and equation (2)

$$\frac{F_b}{F_c} = \frac{\Delta\rho g h_{\text{sample}} r_{\text{throat}}}{2\sigma \cos(\theta)} \quad (2)$$

in which $\frac{F_b}{F_c}$ is the buoyancy over capillary force balance, $\Delta\rho$ is density difference between the fluids ($\rho_{\text{oil}} - \rho_{\text{brine}}$), when the density difference is negative, F_b points in the opposite direction as g (gravitational acceleration), h_{sample} is length of the longest connected cluster, chosen equal to the height of the sample, r_{throat} is radius of the throat, σ is interfacial tension between the fluids, and θ is the contact angle measured through the denser phase.

From Figure 7, it becomes apparent that buoyancy does not play a role of significance in the pore space of Ketton, not even for clusters spanning the length of the complete sample, regardless the wettability state and the pore size. However, when considering oil on the outside of the sample, be it as a droplet sticking out of the sample (Figures 5a, 5c, or 6c) or as a layer covering the surface as in Figure 6b, buoyancy may become important.

4. Conclusions

Spontaneous imbibition was studied using multiscale X-ray computed tomography technique, where small samples (few centimeters in size) were imaged at pore-scale resolution, between 6.7- and 14.25- μm voxel

resolution. The results question the standard Darcy-scale interpretation of such experiments, which are used to assess the wettability state of rock based on production as a function of time. Our results clearly indicate that the curves of cumulative production of the out flowing phase over time do not always reflect the wettability state well. For water-wet core plug samples, the macroscopically obtained production curve matched the observed pore-scale displacement. However, for mixed-wet core plug systems this was not the case: more fluid was exchanged than could be accounted for based on the segmented pore-scale images, which could lead to inaccuracy in the determined wettability state.

Complementing production curves with pore-scale information of the core plug samples did provide a clear qualitative indication of wettability state: water-wet systems show a clear imbibition front, whereas mixed-wet systems do not. A complementary observation in water-wet core plug samples was that the imbibition front had a distinctive asymmetrical character, which may be caused by the presence of preferential production sites.

This mismatch in pore-scale displacement and macroscopic fluid production in mixed-wet core plug samples is thought to be a consequence of a step in the standard experimental protocol in which a sample is rolled over a wetted tissue to remove excess of the fluids from the sample surface.

Therefore, this fluids can account for the excess production we found in the production curves for mixed-wet core plug. If initially a fluid film of approximately 0.25 mm is covering the sample perimeter, excluding top and bottom surfaces, and is fully recovered upon submersion, this would be enough to explain an additional production of 1 ml of oil.

The preferential production sites for all water-wet samples, the existence of oil films following a gradient on the sample surface, and the large drops forming on top of both water-wet and mixed-wet Darcy-scale samples all indicate that buoyancy may play a dominant role for this three-phase system. Computations support this finding for oil protruding from the sample, which is enhanced by an increased gravity head because of the increased connectivity via the external oil film. Pore-scale images of the water-wet miniplug support these findings by showing buoyancy-aided snap-off and spontaneous imbibition in pores adjacent to the sample perimeter.

Our study has wider implications. It demonstrates the value, necessity, and feasibility of combining standard Darcy-scale experiments with pore-scale information acquired by X-ray microcomputed tomography on benchtop laboratory equipment. This makes it possible to resolve the natural length and time scale of the underlying processes in multiphase flow in general and spontaneous imbibition in particular. It is expected that the domain of pore-scale experimentation and traditional disciplines such as special core analysis will merge in this way. This study is the first concrete manifestation of this new trend, demonstrated on a problem of practical relevance.

Acronyms

FOV	Field of View
FW	Formation Water
IFT	Interfacial Tension
MICP	Mercury Injection Capillary Pressure
NAPL	Nonaqueous Phase Liquid
PEEK	PolyEther Ether Ketone
SCAL	Special Core Analysis
TAN	Total Acid Number
TBN	Total Base Number
TDS	Total Dissolved Solids

References

- Alava, M., Dubé, M., & Rost, M. (2004). Imbibition in disordered media. *Advances in Physics*, 53(2), 83–175.
- Alizadeh, S. M., Latham, S., Middleton, J., Limaye, A., Senden, T. J., & Arns, C. H. (2017). Regional analysis techniques for integrating experimental and numerical measurements of transport properties of reservoir rocks. *Advances in Water Resources*, 100, 48–61.
- Amott, E. (1959). Observations relating to the wettability of porous rock. *Petroleum Transactions AIME*, 216, 156–162.
- Anderson, W. G. (1987). Wettability literature survey-part 5: The effects of wettability on relative permeability. *Journal of Petroleum Technology*, 39(11), 1–453.

Acknowledgments

Data are available online from Bartels et al. (2019, <https://www.digitalrockportal.org/projects/188>, DOI: 10.17612/P7M96P). We would like to acknowledge the staff of UGCT, Ghent, Belgium, for support during the execution of this work. We thank Alex Schwing and Rob Neiteler for the creation of the flow setup and instrumentation, Fons Marcelis and Ab Coorn for sample preparation, and Kamaljit Singh from Imperial College London for supplying the Ketton rock. Ali Fadili is thanked for the Shell internal technical review and Christopher Zahasky for helpful discussions regarding the stability of the imbibition front.

- Andrew, M., Bijeljic, B., & Blunt, M. J. (2014a). Pore-scale contact angle measurements at reservoir conditions using X-ray microtomography. *Advances in Water Resources*, *68*, 24–31.
- Andrew, M., Bijeljic, B., & Blunt, M. J. (2014b). Pore-by-pore capillary pressure measurements using X-ray microtomography at reservoir conditions: Curvature, snap-off, and remobilization of residual CO₂. *Water Resources Research*, *50*, 8760–8774. <https://doi.org/10.1002/2014WR015970>
- Armstrong, R. T., Georgiadis, A., Ott, H., Klemin, D., & Berg, S. (2014). Critical capillary number: Desaturation studied with fast X-ray computed microtomography. *Geophysical Research Letters*, *41*, 55–60. <https://doi.org/10.1002/2013GL058075>
- Armstrong, R. T., Pentland, C. H., Berg, S., Hummel, J., Lichau, D., & Bernard, L. (2012). Estimation of curvature from micro-CT liquid-liquid displacement studies with pore scale resolution. In *International Symposium of the Society of Core Analysts held in Aberdeen, Scotland, UK, 27-30 August 2012*, SCA2012–55.
- Armstrong, R. T., Porter, M. L., & Wildenschild, D. (2012). Linking pore-scale interfacial curvature to column-scale capillary pressure. *Advances in Water Resources*, *46*, 55–62.
- Bartels, W.-B., Rücker, M., Boone, M., Bultreys, T., & Cnudde, V. (2019). Micro-CT datasets for spontaneous imbibition experiments on SCAL and mini-plugs. Retrieved from: Digital Rocks Portal, <https://www.digitalrockportal.org/projects/188>, <https://doi.org/10.17612/P7M96P>
- Berg, S., Armstrong, R. T., Ott, H., Georgiadis, A., Klapp, S. A., Schwing, A., et al. (2014). Multiphase flow in porous rock imaged under dynamic flow conditions with fast X-ray computed microtomography. *Petrophysics*, *55*(04), 304–312.
- Berg, S., Oedai, S., & Ott, H. (2013). Displacement and mass transfer between saturated and unsaturated CO₂/brine systems in sandstone. *International Journal of Greenhouse Gas Control*, *12*, 478–492.
- Bickle, M. J. (2009). Geological carbon storage. *Nature Geoscience*, *2*(12), 815.
- Blunt, M. J. (2001). Flow in porous media: Pore-network models and multiphase flow. *Current Opinion in Colloid & Interface Science*, *6*(3), 197–207.
- Blunt, M. J., Jackson, M. D., Piri, M., & Valvatne, P. H. (2002). Detailed physics, predictive capabilities and macroscopic consequences for pore-network models of multiphase flow. *Advances in Water Resources*, *25*(8-12), 1069–1089.
- Brusseau, M. L. (1992). Rate-limited mass transfer and transport of organic solutes in porous media that contain immobile immiscible organic liquid. *Water Resources Research*, *28*(1), 33–45.
- Bultreys, T., Boone, M. A., Boone, M. N., De Schryver, T., Masschaele, B., Van Hoorebeke, L., & Cnudde, V. (2016). Fast laboratory-based micro-computed tomography for pore-scale research: Illustrative experiments and perspectives on the future. *Advances in Water Resources*, *95*, 341–351.
- Bultreys, T., Boone, M. A., Boone, M. N., De Schryver, T., Masschaele, B., Van Loo, D., et al. (2015). Real-time visualization of haines jumps in sandstone with laboratory-based microcomputed tomography. *Water Resources Research*, *51*, 8668–8676. <https://doi.org/10.1002/2015WR017502>
- Bultreys, T., De Boever, W., & Cnudde, V. (2016). Imaging and image-based fluid transport modeling at the pore scale in geological materials: A practical introduction to the current state-of-the-art. *Earth-Science Reviews*, *155*, 93–128.
- Cai, J., You, L., Hu, X., Wang, J., & Peng, R. (2012). Prediction of effective permeability in porous media based on spontaneous imbibition effect. *International Journal of Modern Physics C*, *23*(7), 1250054.
- Chaudhary, K., Bayani Cardenas, M., Wolfe, W. W., Maisano, J. A., Ketcham, R. A., & Bennett, P. C. (2013). Pore-scale trapping of supercritical CO₂ and the role of grain wettability and shape. *Geophysical Research Letters*, *40*, 3878–3882. <https://doi.org/10.1002/grl.50658>
- Cnudde, V., & Boone, M. N. (2013). High-resolution X-ray computed tomography in geosciences: A review of the current technology and applications. *Earth-Science Reviews*, *123*, 1–17.
- De Kock, T., Boone, M. A., De Schryver, T., Van Stappen, J., Derluyn, H., Masschaele, B., et al. (2015). A pore-scale study of fracture dynamics in rock using X-ray micro-CT under ambient freeze-thaw cycling. *Environmental Science & Technology*, *49*(5), 2867–2874.
- De Rooij, G. H. (2000). Modeling fingered flow of water in soils owing to wetting front instability: A review. *Journal of Hydrology*, *231*, 277–294.
- Dierick, M., van Loo, D., Masschaele, B., van den Bulcke, J., van Acker, J., Cnudde, V., & van Hoorebeke, L. (2014). Recent micro-CT scanner developments at UGCT. *Nuclear Instruments and Methods in Physics Research B*, *324*, 35–40.
- Dixit, A. B., Buckley, J. S., McDougall, S. R., & Sorbie, K. S. (1999). Core wettability: Should IAH equal IUSBM. *Petroleum Transactions AIME*, SCA9809.
- Donaldson, E. C., Thomas, R. D., & Lorenz, P. B. (1969). Wettability determination and its effects on recovery efficiency. *SPE Journal*, *9*(01), SPE-2338-PA. <https://doi.org/10.2118/2338-PA>
- Fernø, M. A., Haugen, A., Brattekas, B., Morrow, N. R., & Mason, G. (2015). Spontaneous imbibition revisited—a new method to determine KR and PC by inclusion of the capillary backpressure. In *IOR 2015-18th European symposium on improved oil recovery*, Dresden, Germany.
- Fischer, H., & Morrow, N. R. (2005). Spontaneous imbibition with matched liquid viscosities. In *SPE annual technical conference and exhibition, held in Dallas, Texas, USA from 9–12 October 2005*. SPE 96812. <https://doi.org/10.2118/96812-MS>
- Graue, A., Aspenes, E., Bogno, T., Moe, R. W., & Ramsdal, J. (1999). Alteration of wettability and wettability heterogeneity. *Journal of Petroleum Science and Engineering*, *33*, 3–17.
- Gruener, S., Sadjadi, Z., Hermes, H. E., Kityk, A. V., Knorr, K., Egelhaaf, S. U., et al. (2012). Anomalous front broadening during spontaneous imbibition in a matrix with elongated pores. *Proceedings of the National Academy of Sciences*, *109*(26), 10245–10250.
- Haugen, Å., Fernø, M. A., Mason, G., & Morrow, N. R. (2014). Capillary pressure and relative permeability estimated from a single spontaneous imbibition test. *Journal of Petroleum Science and Engineering*, *115*, 66–77.
- Huang, D. D., & Honarpour, M. M. (1998). Capillary end effects in coreflood calculations. *Journal of Petroleum Science and Engineering*, *19*(1-2), 103–117.
- Juanes, R., Spiteri, E., Orr Jr, F., & Blunt, M. (2006). Impact of relative permeability hysteresis on geological CO₂ storage. *Water Resources Research*, *42*, W12418. <https://doi.org/10.1029/2005WR004806>
- Kovscek, A. R., Wong, H., & Radke, C. J. (1993). A pore-level scenario for the development of mixed wettability in oil reservoirs. *AIChE Journal*, *39*(6), 1072–1085.
- Lee, H., Yeo, I. W., & Lee, K. (2007). Water flow and slip on NAPL-wetted surfaces of a parallel-walled fracture. *Geophysical Research Letters*, *34*, L19401. <https://doi.org/10.1029/2007GL031333>
- Lv, P., Liu, Y., Wang, Z., Liu, S., Jiang, L., Chen, J., & Song, Y. (2017). In situ local contact angle measurement in a CO₂-brine-sand system using microfocused X-ray CT. *Langmuir*, *33*(14), 3358–3366.

- Ma, S., Morrow, N. R., & Zhang, X. (1997). Generalized scaling of spontaneous imbibition data for strongly water-wet systems. *Journal of Petroleum Science and Engineering*, *18*, 165–178.
- March, R., Doster, F., & Geiger, S. (2016). Accurate early-time and late-time modeling of countercurrent spontaneous imbibition. *Water Resources Research*, *52*, 6263–6276. <https://doi.org/10.1002/2015WR018456>
- Mason, G., Fischer, H., Morrow, N. R., Johannesen, E., Haugen, A., Graue, A., & Fernø, M. A. (2010). Oil production by spontaneous imbibition from sandstone and chalk cylindrical cores with two ends open. *Energy & Fuels*, *24*(2), 1164–1169.
- Mason, G., Fischer, H., Morrow, N. R., & Ruth, D. W. (2009). Spontaneous counter-current imbibition into core samples with all faces open. *Transport in Porous Media*, *78*(2), 199–216.
- Mason, G., & Morrow, N. R. (2013). Developments in spontaneous imbibition and possibilities for future work. *Journal of Petroleum Science and Engineering*, *110*, 268–293.
- Mattax, C. C., & Kyte, J. R. (1962). Imbibition oil recovery from fractured water-drive reservoir. *Society of Petroleum Engineers Journal*, *2*(02), 177–184.
- Miranda, A. M., Menezes-Sobrinho, I. L., & Couto, M. S. (2010). Spontaneous imbibition experiment in newspaper sheets. *Physical review letters*, *104*(8), 86101.
- Morrow, N. R. (1975). The effects of surface roughness on contact: Angle with special reference to petroleum recovery. *Journal of Canadian Petroleum Technology*, *14*(4), 42–53. <https://doi.org/10.2118/75-04-04>
- Morrow, N. R., Lim, H. T., & Ward, J. S. (1986). Effect of crude-oil-induced wettability changes on oil recovery. *SPE Formation Evaluation*, *1*(1), 89–103.
- Muir-wood, H. M. (1952). Some jurassic brachiopoda from the lincolnshire limestone and upper estuarine series of rutland and lincolnshire. *Proceedings of the Geologists' Association*, *63*(2), 113–142.
- O'Carroll, D. M., Mumford, K. G., Abriola, L. M., & Gerhard, J. I. (2010). Influence of wettability variations on dynamic effects in capillary pressure. *Water Resources Research*, *46*, W08505. <https://doi.org/10.1029/2009WR008712>
- Picchi, D., & Battiato, I. (2018). Relative permeability scaling from pore-scale flow regimes. *Water Resources Research*, *55*, 3215–3233. <https://doi.org/10.1029/2018WR024251>
- Powers, S. E., Anckner, W. H., & Seacord, T. F. (1996). Wettability of napl-contaminated sands. *Journal of Environmental Engineering*, *122*(10), 889–896.
- Rücker, M., Bartels, W.-B., Singh, K., Brussee, N., Coorn, A., van der Linde, H. A., et al. (2019). The effect of mixed wettability on pore-scale flow regimes based on a flooding experiment in ketton limestone. *Geophysical Research Letters*, *46*, 3225–3234. <https://doi.org/10.1029/2018GL081784>
- Salathiel, R. A. (1973). Oil recovery by surface film drainage in mixed-wettability rocks. *Journal of Petroleum Technology*, *25*, 1216–1224.
- Schmid, K. S., & Geiger, S. (2012). Universal scaling of spontaneous imbibition for water-wet systems. *Water Resources Research*, *48*, W03507. <https://doi.org/10.1029/2011WR011566>
- Schmid, K. S., & Geiger, S. (2013). Universal scaling of spontaneous imbibition for arbitrary petrophysical properties: Water-wet and mixed-wet states and handys conjecture. *Journal of Petroleum Science and Engineering*, *101*, 44–61.
- Suijkerbuijk, B. M. J. M., Kuipers, H., Van Kruijsdijk, C., Berg, S., Van Winden, J. F., Ligthelm, D. J., et al. (2013). The development of a workflow to improve predictive capability of low salinity response. In *IPTC 2013: International Petroleum Technology Conference*, Beijing, China.
- Tang, G. Q., & Morrow, N. R. (1997). Salinity, temperature, oil composition, and oil recovery by waterflooding. *SPE Journal*, *12*(04), SPE-36680-PA. <https://doi.org/10.2118/36680-PA>.
- Unsal, E., Mason, G., Morrow, N. R., & Ruth, D. W. (2009). Bubble snap-off and capillary-back pressure during counter-current spontaneous imbibition into model pores. *Langmuir*, *25*(6), 3387–3395.
- Unsal, E., Mason, G., Morrow, N. R., & Ruth, D. W. (2007). Co-current and counter-current imbibition in independent tubes of non-axisymmetric geometry. *Journal of colloid and interface science*, *306*(1), 105–117.
- Unsal, E., Mason, G., Ruth, D. W., & Morrow, N. R. (2007). Co-and counter-current spontaneous imbibition into groups of capillary tubes with lateral connections permitting cross-flow. *Journal of Colloid and Interface Science*, *315*(1), 200–209.
- Van Stappen, J., De Kock, T., Boone, M., Olaussen, S., & Cnudde, V. (2014). Pore-scale characterization and modelling of CO₂ flow in tight sandstones using X-ray micro-CT; Knorringfjellet formation of the Longyearbyen CO₂ lab, Svalbard. *Norwegian Journal of Geology*, *94*(2-3), 201–215.
- Wang, Y., & Masalmeh, S. K. (2019). Obtaining high quality scal data: Combining different measurement techniques, saturation monitoring, numerical interpretation and continuous monitoring of experimental data. *E3S Web Conferences*, *89*, 2007.
- Weisbrod, N., McGinnis, T., Rockhold, M. L., Niemet, M. R., & Selker, J. S. (2009). Effective darcy-scale contact angles in porous media imbibing solutions of various surface tensions. *Water Resources Research*, *45*, W00D39. <https://doi.org/10.1029/2008WR006957>
- Xiong, Y. (2014). Flow of water in porous media with saturation overshoot: A review. *Journal of Hydrology*, *510*, 353–362.
- Zahasky, C., & Benson, S. M. (2019). Spatial and temporal quantification of spontaneous imbibition. Preprint on <https://essoar.org> (2018). <https://doi.org/10.1002/essoar.10501010.1>
- Zhou, X., Morrow, N. R., & Ma, S. (2000). Interrelationship of wettability, initial water saturation, aging time and oil recovery by spontaneous imbibition and waterflooding. *SPE Journal*, *5*(2), 199–207.
- Zou, S., Armstrong, R. T., Arns, J., Arns, C. H., & Hussain, F. (2018). Experimental and theoretical evidence for increased ganglion dynamics during fractional flow in mixed-wet porous media. *Water Resources Research*, *54*, 3277–3289. <https://doi.org/10.1029/2017WR022433>